Journal of Alloys and Compounds 638 (2015) 356–363

Contents lists available at ScienceDirect

Journal of Alloys and Compounds

journal homepage: www.elsevier.com/locate/jalcom

Influence of annealing temperature on structural and optical properties of SiO_2:RE_2O_3 [RE = Y, Gd] powder

Rachna Ahlawat *

Department of Physics, Materials Science Lab., Ch. Devi Lal University, Sirsa 125055, Haryana, India

ARTICLE INFO

Article history:
Received 16 December 2014
Received in revised form 2 March 2015
Accepted 9 March 2015
Available online 20 March 2015

Keywords:
Binary oxide
Four step annealing
Structural properties
Optical properties

ABSTRACT

SiO_2:RE_2O_3 [RE = Y, Gd] powder were prepared by wet chemical technique and the prepared binary oxides annealed at 500 °C and 900 °C. The crystalline structure, phase transformation, and surface morphologies of as-prepared and annealed samples were investigated by XRD and TEM. The normal transmission was measured using FTIR spectroscopy. Optical properties have been studied with UV–Vis spectroscopy and PL study. XRD results shows that the as prepared samples of SiO_2:RE_2O_3 [RE = Y, Gd] powder has mixed phases of $RE(NO_3)_3$ and $Si(OH)_3$. However, cubic rare earth oxide phase alone is found for annealed samples. The strain values are calculated from W–H plot for annealed samples. TEM micrograph shows that the samples are composed of individual spherical nanocrystallites at 500 °C and aggregated nanocrystallites at 900 °C. From the UV–Vis spectra, it is found that the position of the absorption peak is shifted toward the higher wavelength side when annealing temperature is increased. In the PL spectra, the broad emission bands are observed between 570–600 nm and the presence of O–Si–O (silica) and metal oxide is confirmed by FTIR spectra.

1. Introduction

Powder, ceramic and composites of oxides in the nanometer size have received much attention due to their various properties and they significantly used in fundamental and application oriented fields. Since oxide nanoparticles are having very large surface area, they are used in catalytic applications [1]. These particles are acting as a sensor to detect the various gases present in the environment and also help to reduce the air pollution [2]. Oxide nanoparticles embedded in a polymer matrix produce nanocomposites which are useful for electronic applications [3]. From the basic physics point of view, these compounds exhibit interesting optical, magnetic and electronic properties with potential applications either as powder or thin film like compact fluorescent lamps, light emitting diodes, plasma display panels, high definition televisions, in biomedical applications, as sensors, as IR windows, nano heaters, and latent fingerprint detection [4–6]. Also, rare earth oxides are used as high index oxide for dielectric mirror for high powered lasers, refractory and ceramic material for industries [7–9].

In last decades, binary system containing nanocrystallites RE_2O_3 (RE, rare earth-Y, Gd) containing SiO_2 are important in various fields of technology, including laser, optoelectronics, microelectronics, optical fiber and photonics, etc. [5,7]. In case of photonics applications, silica with its high softening temperature, higher thermal shock resistance, and lower index of refraction than the other oxide glasses, may be an ideal host matrix for the rare earth elements and their oxides.

For the development of powder technology, in particular, demands as a building blocks due to the increase in structural and compositional complexity so that they can be produced with ease, in abundance, at low cost and low temperature. The application of nanocrystalline materials as a powder feedstock for thermal spraying has been facilitated with a wide range of powder sources such as vapor condensation, combustion synthesis, thermo chemical synthesis, and co-precipitation and mechanical alloying/milling and sol–gel process. Among the various powder sources, sol–gel process has the advantage of lower temperature, possibility of making a finely dispersed powder, easy to make and at low cost [10]. Cannas et al. [11] used sol–gel method to prepare Y_2O_3–SiO_2, after thermal treatment of samples at moderate temperature $T \sim 900$ °C (0.5 h) and high temperature 1300 °C (0.5 h) in air. They found Y_2O_3–SiO_2 as an amorphous when it was sintered at moderate temperature. In another case, Xiaoyi and Yuchun [12] used co-precipitation technique to synthesize Y_2O_3/SiO_2 samples around $T \sim 800$ °C. Sahoo et al. [13] investigated that composite film of SiO_2:Gd_2O_3 have shown superior micro-structure and morphological properties as compared to that of pure thin film. Martino et al. [14] have tried to investigate the effect of concentration on the

* Mobile: +91 9466349170.
E-mail address: rachnaahlawat2003@yahoo.com

http://dx.doi.org/10.1016/j.jallcom.2015.03.077
0925-8388/

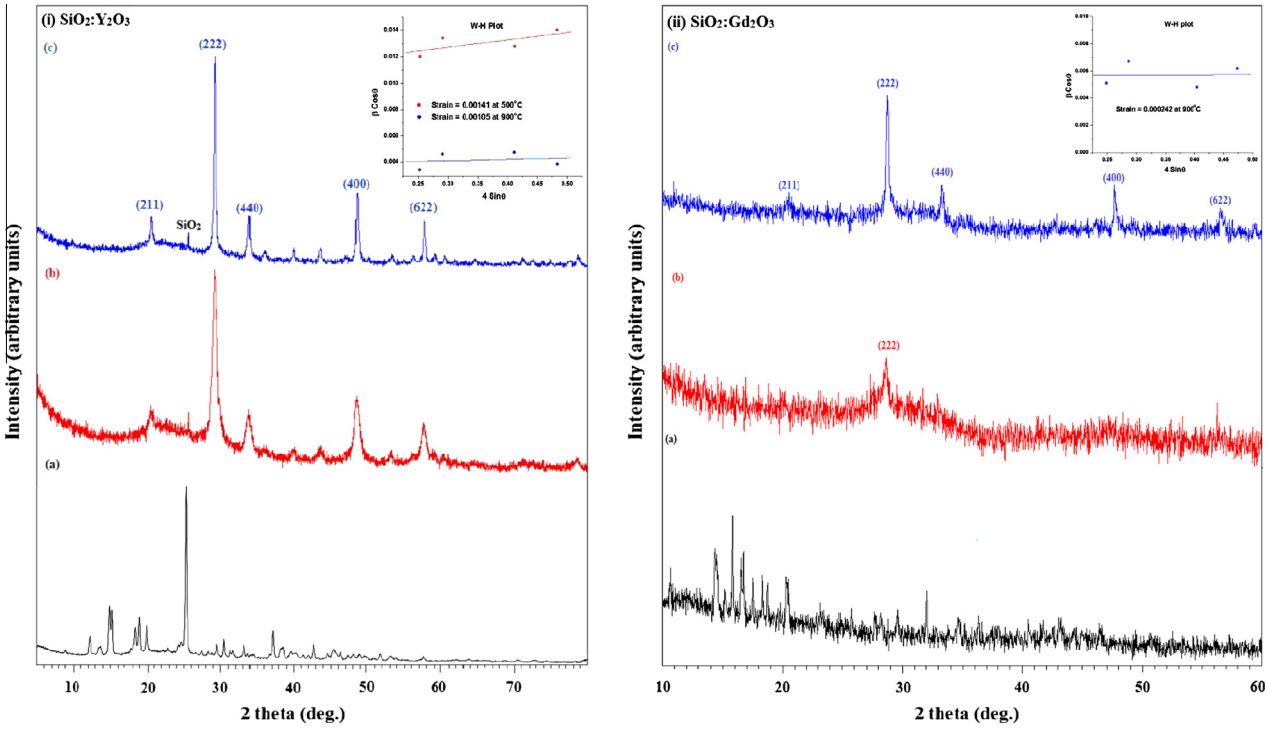

Fig. 1. XRD pattern of (i) SiO_2:Y_2O_3 and (ii) SiO_2:Gd_2O_3 powder for (a) as-prepared, (b) at 500 °C and (c) at 900 °C.

structural properties of gadolinium in sol–gel silica. Zhang et al. [15] have studied comparative bio-effects of SiO_2/Gd_2O_3 nanoparticles depending on their core–shell structures.

Here in the present research work, it is shown that multi-step annealing of SiO_2:RE_2O_3 [RE = Y, Gd] powder at moderate temperature mainly supports the developments of the cubic nanocrystallites. Also, the crystallite size and lattice strain are the two main properties which could be extracted from the peak width analysis. Due to the formation of polycrystalline aggregates, the crystallite size of the particle is not the same as the particle size. Bragg peak is affected by crystallite size and lattice strain which increase the peak width and intensity shifting the 2θ peak position accordingly. The crystallite size varies as $1/\cos\theta$ and stain varies as $\tan\theta$ from the peak width. Williamson–Hall (W–H) analysis is a simplified integral breadth method where both size-induced and strain-induced broadening is determined by considering the peak width as a function of 2θ. Although X-ray profile analysis is an average method, they still hold an unavoidable position for grain size determination, apart from TEM micrographs. In present work, effect of annealing temperature on the structure and the morphology of the nanocrystallites was investigated and discussed in detail. Also, a comparative evaluation of the mean nanocrystallite size of RE_2O_3 obtained from direct TEM measurements, W–H plot and from Debye–Scherrer formula is reported.

The influence of crystallite size on the optical properties was examined using UV–vis absorption spectra and PL studies. Specifically, because of their mechanical strength at high temperature and their thermal shock resistance in combination with their low specific weight, SiO_2:RE_2O_3 [RE = Y, Gd] binary oxides are promising materials for high temperature structural applications.

2. Experimental

2.1. Sample preparation

Powders of Y_2O_3/Gd_2O_3 (99.9%) and SiO_2 (99.9%) were used as starting materials. They were mixed in molar ratio i.e. Si: Y/Gd = 1:6. SiO_2:RE_2O_3 [RE = Y, Gd] powder samples with 4.0 wt% RE_2O_3 content were prepared by sol gel of SiO_2 with an appropriate amount of $Y(NO_3)_3{\cdot}4H_2O$/TEOS and $Gd(NO_3)_3{\cdot}6H_2O$/TEOS (Aldrich 99.9995) precursors. The pH of the solution was kept as 3. The prepared gel was kept at room temperature for 21 days for aging of the samples. In this process initially networking of bonds took place and subsequently with time shrinkage and stiffening of the gel occurred. After aging, the samples were further dried at 100 °C for 24 h and dried samples were powdered by pestle-mortar. The dried sample is named as-prepared (a). Furthermore, the dried samples were annealed in a programmable furnace NSW 103 at several pre-selected temperatures up to 900 °C to study the effect of annealing on structure and optical properties of the powdered samples. In this process, annealing temperatures were elevated in different steps by varying ramp rates (dT/dt) and after each step samples were incubated for few hours. The annealing schedule is shown below:

(a) As-prepared

(b) $R_T \xrightarrow{4C/min} 250°C\,(3h) \xrightarrow{2C/min} 500°C\,(6h)$

(c) $R_T \xrightarrow{6C/min} 250°C\,(3h) \xrightarrow{5C/min} 500°C\,(3h) \xrightarrow{4C/min} 750°C\,(3h) \xrightarrow{2C/min} 900°C\,(6h)$

Table 1
Comparison of size, micro strain and dislocation density.

Sample	(D_{W-H}) (nm)	(D_{D-S}) (nm)	(ε) calculated	$\rho \approx 1/\langle D_{W-H}\rangle^2$ (m^{-2})
(i) SiO_2:Y_2O_3 annealed at 500 °C	13	10	1.41×10^{-3}	5.9×10^{15}
(i) SiO_2:Y_2O_3 annealed at 900 °C	35	33	1.05×10^{-3}	0.82×10^{15}
(ii) SiO_2:Gd_2O_3 annealed at 500 °C	17	15	–	3.5×10^{15}
(ii) SiO_2:Gd_2O_3 annealed at 900 °C	29	27	2.40×10^{-4}	1.2×10^{15}

2.2. Characterizations

As-prepared and annealed samples were characterized by an X'pert Pro X-ray Diffractometer with Cu Kα1 radiation in the range of 5°–80° in steps of 0.017° (40 mA, 45 kV) for the determination of crystalline structure of nanocomposite which were further confirmed by HRTEM Hitachi 4500 micrograph operating at an accelerating voltage of 80 kV. Infrared spectra of as-prepared and annealed samples were collected by Perkin–Elmer Spectrum 400 spectrophotometer in 4000–450 cm^{-1} ranges. For FTIR studies, the samples were mixed homogeneously with KBr and pellets of the desired dimensions made. Specimens for TEM were prepared

by dispersing the powder sample in ethanol and placed a droplet of suspension on a grid coated with perforated carbon. Absorption spectra of the samples were studied with the help of Lambda 750 (Perkin Elmer) spectrophotometer in the wavelength range of 200–600 nm. The photoluminescence (PL) properties of the samples were studied with fluorescence spectrophotometer F-7000 Hitachi having Xenon lamp as its excitation source.

3. Results and discussion

3.1. XRD analysis

Fig. 1 shows the XRD data of powdered SiO_2:RE_2O_3 [RE = Y, Gd] binary oxides. The diffractogram of as-prepared SiO_2:Y_2O_3 and annealed samples are shown in Fig. 1(i). The diffraction pattern of as-prepared sample depicts a very strong and sharp diffraction line centered at $2\theta \sim 25.65°$ and a series of weak peaks between 10° to 45°. These sharp lines of dried sample signify bulk behavior of hydrous precursor's nuclei and this result suggests that the precursors have not decomposed yet. When the temperature was increased up to 500 °C using two step annealing scheme, a strong but slightly broad new peak appeared at $2\theta \sim 29.25°$ along with some weak peaks at $2\theta \sim 20.62°$, 33.85°, 48.58° and 57.77° in the diffraction pattern. The occurrence of these new peaks infers development of a new phase in the sample. In order to identify structure of the polycrystalline phase, "check cell" code was run and found that plane corresponding to diffraction peaks at $2\theta \sim 20.62°$, 33.85°, 48.58°, 57.77° which could be assigned to Miller indices (211), (222), (400), (440) and (622) respectively of the cubic phase of Y_2O_3 with lattice parameter a = 10.56 Å and space group Ia3 (T_h^7) [16,17].

It is expected that multi step annealing scheme reduces the number of pores and their connectivity of the binary oxide around 500 °C and leads to initial crystalline structure in the material [16]. Furthermore, the temperature was raised up to 900 °C to examine structural changes and crystallinity of cubic phase of the powder. A significant increase in intensity and sharpness of the characteristic peaks of Y_2O_3 has been observed which results increase in its crystallinity, densification and size [18]. The increase in intensity of the diffraction peak arises because individual nanostructures merge together and as a result the activation energy becomes larger and therefore grain-boundary diffusion dominates over surface and volume diffusion. Eventually, crystallites start to re-orient in the definite crystallographic directions in order to decrease the deformation strain. In addition the above heat treatment condition yields homogenous morphology of the binary oxides.

Table 2
FTIR peak positions and corresponding functional groups.

Absorption frequency range (cm^{-1})	Modes of vibrations
460–475 cm^{-1}	O–Si–O bending modes [25]
562 and 542 cm^{-1}	Char. vibrational band of Y–O and Gd–O bond [26,27]
803–810 cm^{-1}	Si–O–Si symmetric stretching [25,28]
961–976 cm^{-1}	Silanol group Si–OH [25]
1090–1103 cm^{-1}	Si–O–Si symmetric stretching in cyclic structure (asymmetric stretching) [28]
1476, 1384, 1332 cm^{-1}	Organic residues specially C–O, N–H, NO_3 in ethyl group and nitro group [31]
1625–1650 cm^{-1}	Bending modes of H–O–H adsorbed at silica surface [29]
3450–3390 cm^{-1}	O–H vibrations of residual adsorbed water, Si–OH stretching vibrations [30]

The XRD patterns of as-prepared SiO_2:Gd_2O_3 and annealed samples are shown in Fig. 1(ii). The diffractogram of the as-prepared sample (a) has a sharp and intense diffraction line at $2\theta \sim 15.85°$ along with some weaker peaks at $2\theta \sim 14.44°$, 16.74°, 18.73°, 21.38° and 32.00° which may be assigned to the intermediate phases of gadolinium nitrate hydride compared with JCPDS card no. 84-2385. Sample (a) shows no particular reflection peak corresponding to Gd_2O_3 or SiO_2 in the XRD pattern which indicates that the binary oxide contains only intermediate phases of the precursors.

When the binary system was heated at 500 °C using two steps annealing, significant change in the reflection pattern of the XRD was observed. Sample (b) is not having any peaks of $Gd(NO)_3OH$

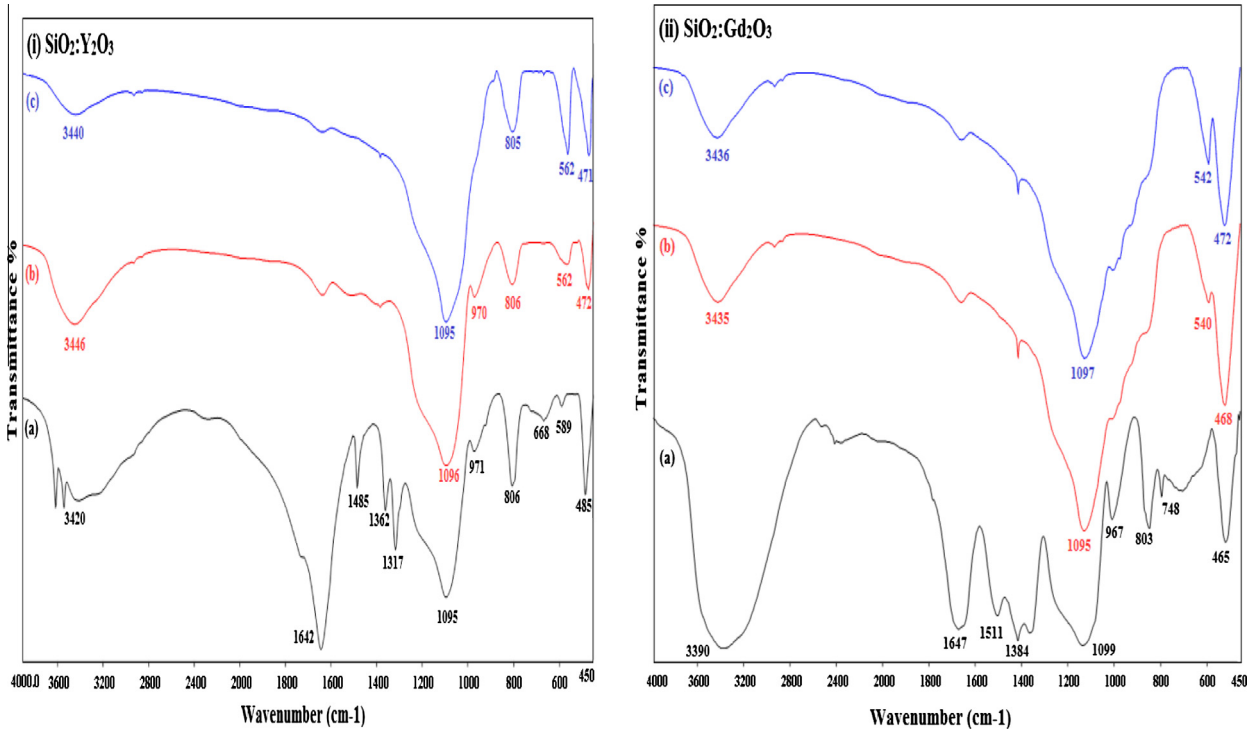

Fig. 2. FTIR spectra of (i) SiO_2:Y_2O_3 and (ii) SiO_2:Gd_2O_3 powder for (a) as-prepared, (b) at 500 °C and (c) at 900 °C.

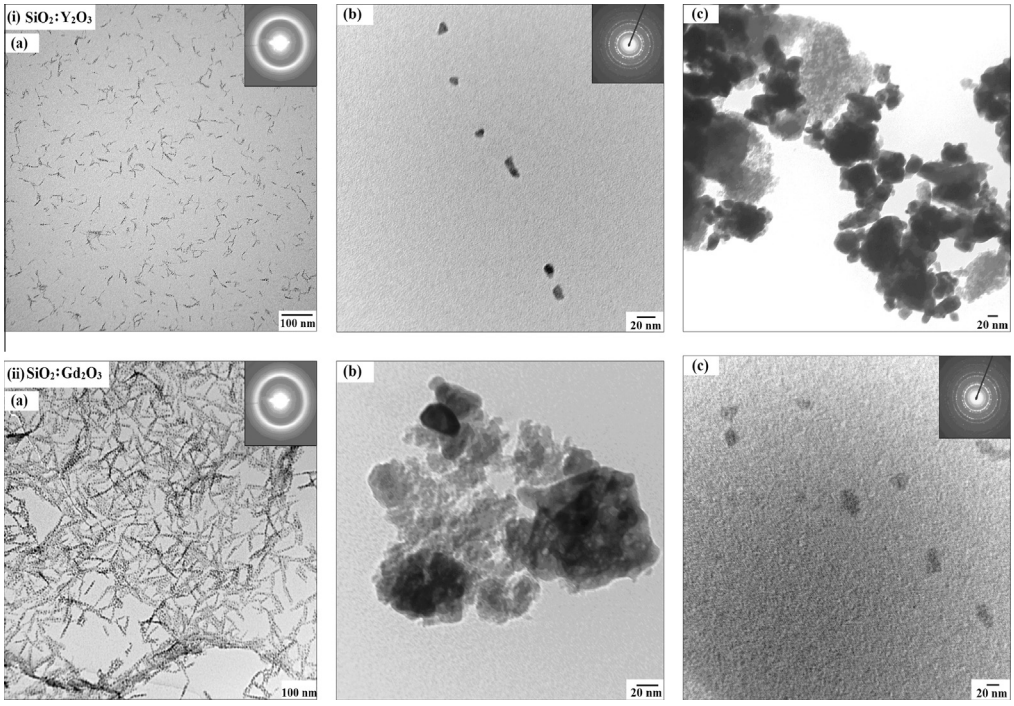

Fig. 3. TEM images of (i) SiO_2:Y_2O_3 and (ii) SiO_2:Gd_2O_3 powder for (a) as-prepared, (b) at 500 °C and (c) at 900 °C.

means precursors are completely decomposed while a small peak at $2\theta \sim 28.66°$ is appeared. This peak manifests that a new phase is going to be develop in the sample. For its identification, temperature was further raised to 900 °C using four step annealing and examined the effect of thermally stored energy on structural behavior of SiO_2: Gd_2O_3 binary oxides. Under this condition, the crystalline structure of the sample may be described by broad reflection centered about $2\theta \sim 28.75°$, 33.31° and 47.70°, respectively. The appeared diffraction peaks are assigned to cubic phase of crystalline Gd_2O_3 having space group Ia3 (206) [JCPDS card no. 43-1014] [19].

The lattice constant of the cubic Gd_2O_3 was also calculated according to the equation: $[1/d^2 = (h^2 + k^2 + l^2)/a^2]$, where d is the interplanar distance, h, k, l are the crystal indices (Miller indices), and a being lattice constant. On the basis of the (222) crystal planes ****(d = 3·1179 Å), the lattice constant a = 10·80 Å is calculated for sol–gel derived cubic Gd_2O_3, which is well compatible with the literature value of a = 10·809(9) Å [20]. Check cell program was used to obtain symmetry of composite and miller indices which were found to be (222), (400), and (440) corresponding to $2\theta \sim 28.75°$, 33.31° and 47.70° respectively.

From XRD measurements, it is concluded that heat treatment using multi steps annealing changes the nature of the sample from amorphous to crystalline and results in the development of single cubic phase along with increased crystallite size and densification.

3.1.1. Nanocrystallite size, strain and dislocation density

The micro-strain and crystallite size produces peak broadening in the diffractogram. The crystallite size and strain effect have to be differentiated in the diffractogram. Both effects are independent and can be distinguished by W–H equation [21,22]:

$$\beta_{hkl}\,\mathrm{Cos}(\theta)_{hkl} = K\lambda/D + 2\,\varepsilon\,\mathrm{Sin}(\theta)_{hkl}$$

where K is the shape factor which is 0.9 for uniform small size crystals, λ is the wavelength of X-ray, θ_{hkl} is the Bragg angle for the (hkl) plane, ε is the micro-strain, β_{hkl} is corrected full width half maximum in radians and D is an average crystallite size for the (hkl) plane measured in a direction perpendicular to the surface of the specimen. A graph is plotted between $\mathrm{Sin}(\theta)_{hkl}$ and $\beta_{hkl}\,\mathrm{Cos}(\theta)_{hkl}$ as shown in the inset of Fig. 1. The value of micro-strain is estimated from slope of the line and the crystallite sizes were obtained from the intersection with the vertical axis which is given in Table 1.

It is noticed that micro-strain reduces gradually with increasing annealing temperature and its influence on broadening XRD peak is negligibly small. Under such considerations ($\varepsilon = 0$), Williamson–Hall relation reduces to Debye–Scherer's formula: $D = K\lambda/\beta\mathrm{Cos}\,\theta$ [23]. The average crystalline size (D) of Gd_2O_3 was also calculated using this formula and the results are compared in Table 1. The mechanism of multi step annealing at higher temperatures can produce dislocations due to irregularities at the grain boundaries in material which propagate into grain. The stored energy is not only proportional to strain but also involves dynamic recovery during deformation. Due to this fact the grain boundaries interfere and eventually atoms or molecules rearrange/reorient in the material. The correlation function between dislocations is assumed to vanish on distances which are of the order of $\rho^{-(2)}$ where ρ is dislocation density. The term $\rho^{-(2)}$ has been interpreted as the 'mean particle size' [24,25]. Using this relationship we found dislocation density of SiO_2:RE_2O_3 [RE = Y, Gd] powder at different temperature. The dislocation density of SiO_2:Y_2O_3 and SiO_2:Gd_2O_3 samples are decreased by 85% and 75%, respectively when the sample was annealed at 900 °C (6 h). In addition, it also suggests that combination of high temperature and prolonged calcinations reduces dislocation density and amount of stress at the surface and hence yields the densification and strength of the materials.

3.2. FTIR analysis

The infrared absorption spectra of the prepared samples provide some important information about the structural changes. The FTIR spectra of as prepared and annealed sample of SiO_2:RE_2O_3 [RE = Y, Gd] binary oxides are shown in Fig. 2(i) and (ii) within the spectral range of 4000–450 cm^{-1}. Table 2 shows

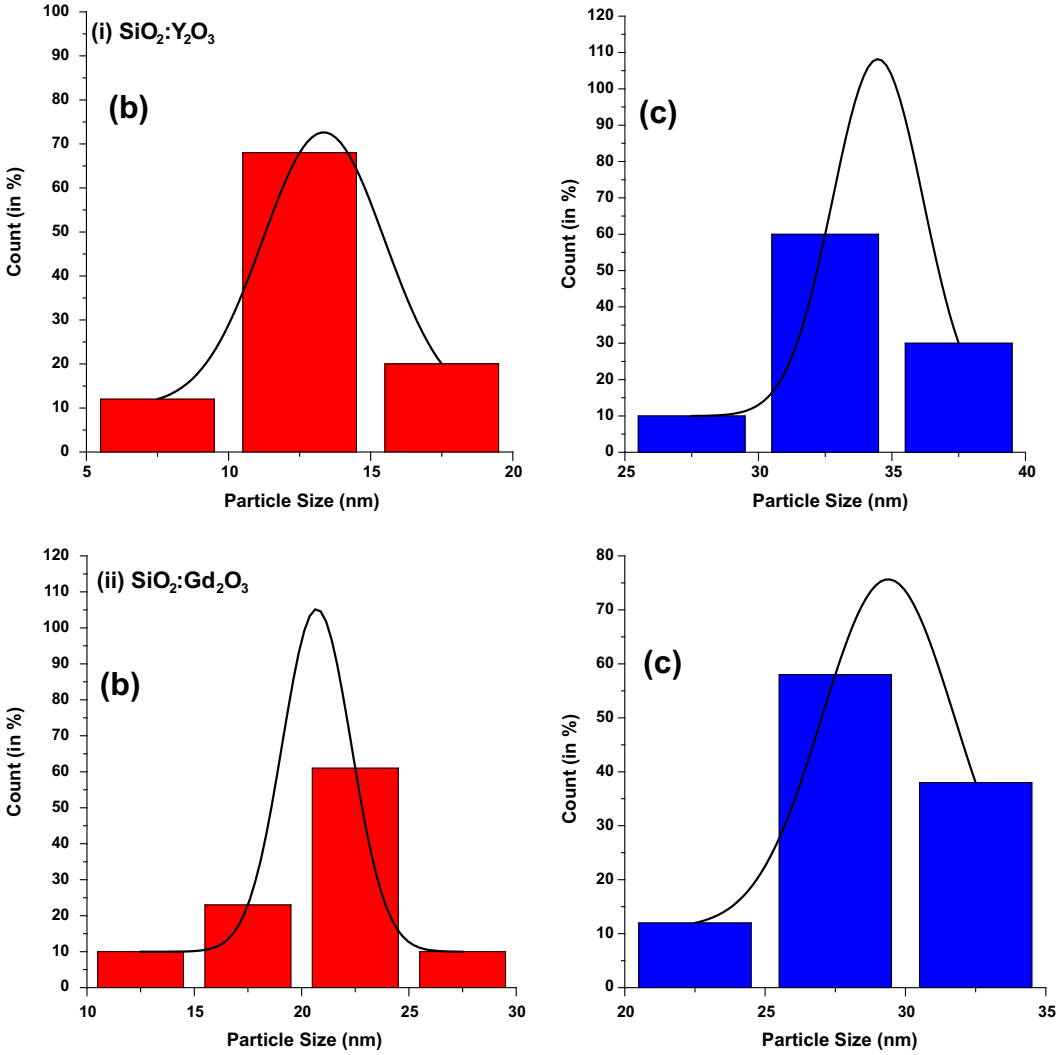

Fig. 4. Particle size distributions of (i) SiO_2:Y_2O_3 and (ii) SiO_2:Gd_2O_3 powder.

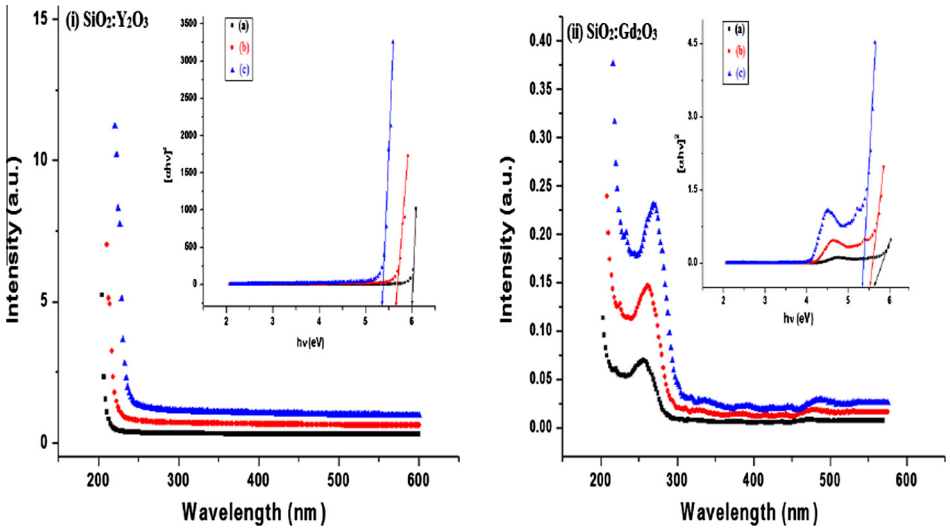

Fig. 5. Absorption spectra and band gap energy of (i) SiO_2:Y_2O_3 and (ii) SiO_2:Gd_2O_3 powder for (a) as-prepared, (b) at 500 °C and (c) at 900 °C.

the sources and absorption bands of the FTIR spectra for all the prepared samples. It is concluded from FTIR spectra that toward the lower wave number side of the sample (b), RE-O (RE-Y, Gd) absorption bands becomes broader compared to sample (c) heated at 900 °C via four step annealing. It is understood that the decrease in the particle size enhances the surface effects which in turn

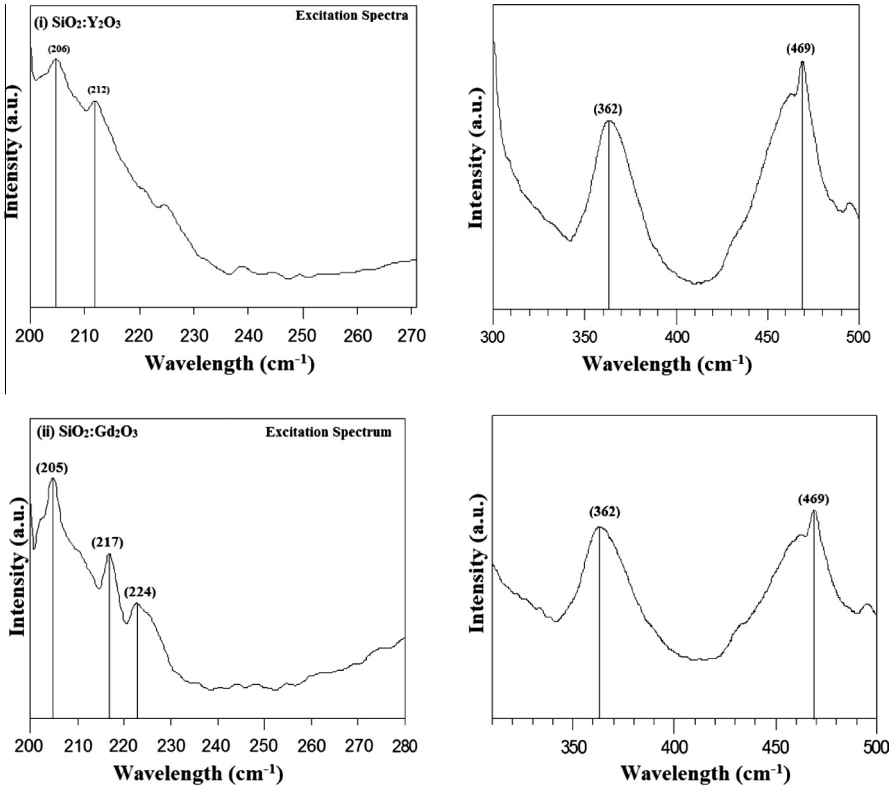

Fig. 6. Photoluminescence excitation spectra of (i) SiO_2:Y_2O_3 and (ii) SiO_2:Gd_2O_3 powder for all samples.

enlarge the absorption. Thus, the RE-O absorption bands are widened. Results of FTIR support the XRD data.

3.3. TEM analysis

The TEM micrographs and Selected Area Electron Diffraction (SAED) pattern of as-prepared and annealed samples of SiO_2:RE_2O_3 [RE = Y, Gd] powder are shown in Fig. 3(i) and (ii). The crystallite size and particle morphology of the as-prepared sample (a) and annealed samples at 500 °C (b) and at 900 °C (c) are observed. The diffused SAED ring pattern is observed for as-prepared samples. The sharp ring pattern observed for annealed sample confirms the crystalline nature of the sample. Micrograph of as prepared sample for SiO_2:Y_2O_3 powder shows a typical chain-like structure of acidic gel of precursors which confirms the acid nature of the precursors. The TEM micrographs of the sample (b) annealed at 500 °C shows non-agglomerated yttria nanocrystallites having size ranges 10–15 nm. These samples contain fine particles which are more or less spherical in shape. The nanocrystals have narrow grain size distribution as shown in Fig. 4(ib). When the temperature of heat treatment was raised, as a result of strong interactions between and high surface energy of nanoparticles, they tend to agglomerate. The TEM micrograph of sample (c) at 900 °C shows the aggregated nature of the nanocrystallites with different shape and sizes. Due to the annealing, aggregation of primary particles produce large nanocrystallites whose average grain sizes have been estimated with the help of Gaussian fit to the histograms shown in Fig. 4(ic). The particle size distribution results in bigger size particles in the range of 25–40 nm; among them 80% crystallites are having size 35–40 nm. Also, four steps annealing at 900 °C results bridges between irregular grains which might hinder further grain growth [32]. The average grain size of the nanocrystallites at 900 °C was calculated ~35 ± 2 nm. These results of TEM are complement and support the XRD and FTIR data.

The TEM micrograph for SiO_2:Gd_2O_3 binary oxide has been shown in Fig. 3(ii) which is further confirm the homogenous distribution of gadolinium oxide in silica and grain growth process. Here, one may notice that the as-prepared sample is not of crystalline in nature. Two steps annealing in sample (b) at 500 °C produced nanocrystallites which are having size ranges in 20–25 nm, with quite narrow size distribution, as shown in Fig. 4(iib). The grain growth at 500 °C indicates the high diffusivity of grain boundary of obtained nanocrystallites with in the silica matrix. The average grain size of the sample (b) was calculated ~22 ± 2 nm using Gaussian fit to the corresponding histograms. The nanocrystallites of gadolinium oxide annealed via four steps at 900 °C are homogenously dispersed in silica and having almost spherical shapes. Further, the histogram shown in Fig. 4(iic) indicates that the nanocrystallites annealed at 900 °C gradually grew into larger spherical nanocrystallites having size ranges in 25–30 nm. The average grain size of the SiO_2:Gd_2O_3 nanocrystallite at 900 °C was calculated ~27 ± 2 nm.

Therefore, the TEM results suggest that the four step annealing of rare earth containing silica supports coalescence of the individual nanocrystals. In case of SiO_2:RE_2O_3 [RE = Y, Gd] powder such heat treatment mainly supports formation of the cubic phase of spherical nanocrystallites over the other phases with high densification of the prepared binary oxides.

3.4. Optical absorption and band gap energy

The absorption spectra for SiO_2:Y_2O_3 has been shown in Fig. 5(i) and its band gap energy in displayed in the inset of the same figure. The absorption peak for as-prepared sample (a) occurred at 206 and 212 nm which lies at lower wavelength (blue shift) side as compared with bulk form of Y_2O_3 [33]. It is also observed that the absorption edge of the samples has shifted toward lower energy side (red shift) as the annealing temperature was increased.

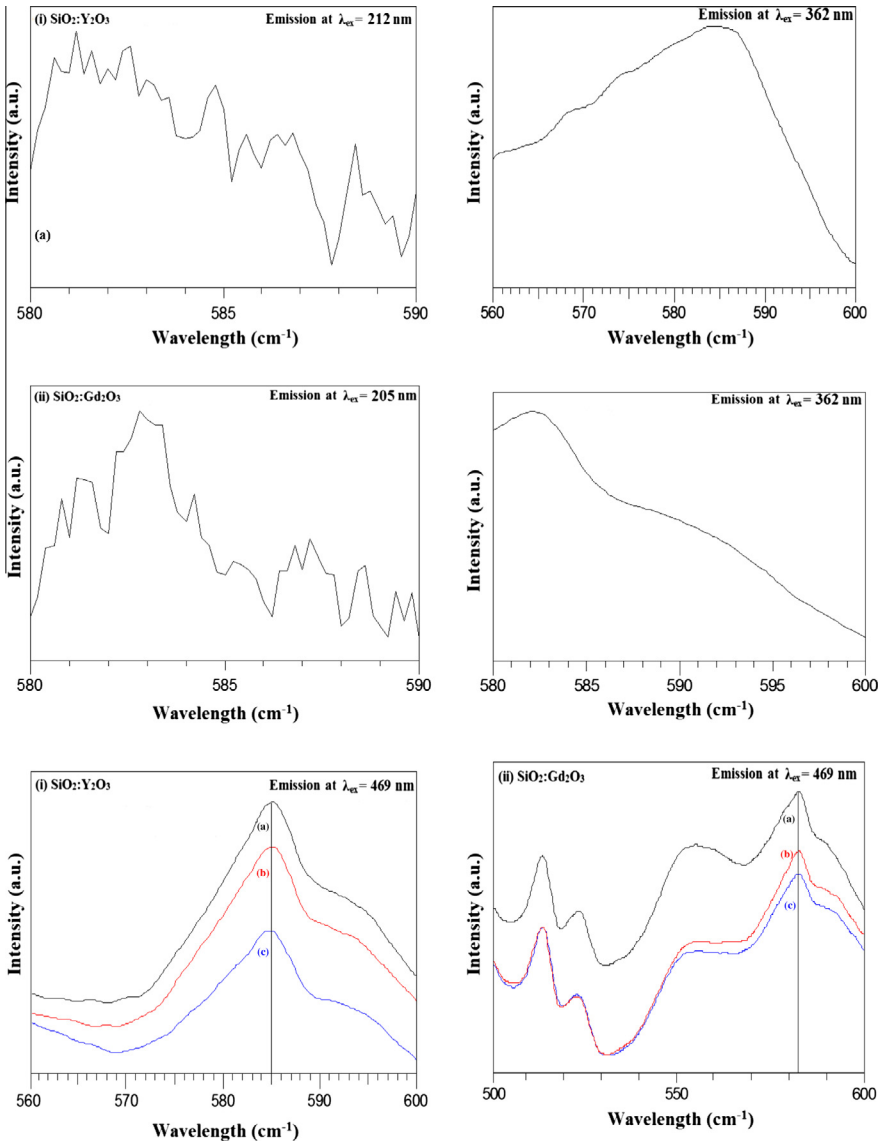

Fig. 7. Photoluminescence emission spectra of (i) SiO_2:Y_2O_3 and (ii) SiO_2:Gd_2O_3 powder for (a) as-prepared, (b) at 500 °C and (c) at 900 °C.

The band gap energy of as-prepared and annealed samples has been calculated using the relation between the incident photon energy ($h\nu$) and the absorption coefficient (α) which is given by the equation: $(\alpha h\nu)^{1/n} = A\,(h\nu - E_g)$, where α is a constant and E_g is the band gap energy of the material and the exponent n depends on the type of transition [34]. Direct band gap of the samples (using $n = ½$) were calculated by plotting $(\alpha h\nu)^2$ verses $h\nu$ and then extrapolating the straight portion of the curve on $h\nu$ axis at $\alpha = 0$ as shown in inset of Fig. 5(i). The band gap energy for samples (a), (b), and (c) is estimated as 6.0, 5.65 and 5.40 eV respectively.

The optical absorption spectra of SiO_2:Gd_2O_3 powder for as prepared and the annealed samples are shown in Fig. 5(ii). The absorption peaks observed at 220 and 265 nm in as-prepared sample, which shift toward higher wavelength side with temperature. Therefore, there exists blue shift in the absorption spectra of as-prepared sample as compared to bulk form of gadolinium oxide and red shift occurs with annealing temperature. It is found that blue shift has been occurred due to well known quantum size effect [35]. The possible reason for red shift in band-gap energy with annealing temperature could be aggregation effects, strongest interaction of rare earth oxide in solid state and specially ascribed to band tail effects [36]. The band gap energies of sample (a), (b) at 500 °C and (c) at 900 °C is calculated as 5.60, 5.50 and 5.45 eV, respectively.

3.5. Photoluminescence

The photoluminescence excitation spectra were observed at room temperature in two spectral regions, first in the range 200–280 nm and second in 300–500 nm which has been shown in Fig. 6. It can be seen from Fig. 6(i) that a small peak is appeared around ~212 nm in the excitation spectrum of SiO_2:Y_2O_3 binary oxide observed in the first spectral region which could be used as an excitation wavelength for the emission spectra. However, the excitation spectrum in 300–500 nm regions consisted of two main peaks centered at 362 and 469 nm for the as prepared samples (a) as shown in Fig. 6(i) for SiO_2:Y_2O_3 and Fig. 6(ii) for SiO_2:Gd_2O_3. All these excitation wavelengths have been used for observing the emission spectra of the corresponding samples (a), (b) and (c).

In this research work, we have observed the emission spectra of SiO_2:Y_2O_3 and SiO_2:Gd_2O_3 powder for all the possible excitation wavelengths. Fig. 7(i) shows the emission spectrum observed at $\lambda_{ex} = 212$ nm for SiO_2:Y_2O_3 powder which is found well in

agreement with those reported by Xiaoyi and Yuchun [12]. The emission spectrum corresponding to λ_{ex} = 362 nm is also shown in this figure which is not completely Gaussian in shape. The photoluminescence emission observed at λ_{ex} = 212 and 362 nm has been centered at 585 nm. The complete Gaussian but broad emission spectra of as-prepared and annealed samples of SiO_2:Y_2O_3 powder has been observed corresponding to excitation wavelength $\lambda_{ex} \sim 469$ nm which is also shown in Fig. 7(i). The observed emission band is centered at 585 nm in the spectral region of 570–600 nm.

The photoluminescence (PL) of the SiO_2:Gd_2O_3 samples have been obtained for all the possible excitation wavelengths and at the identical testing with SiO_2:Y_2O_3. The emission spectrum has main band centered at 583 nm in the spectral region 580–590 nm corresponding to λ_{ex} = 205, 362 and 469 nm. It is expected that the emission bands centered at 583 nm for sample (ii) shown in Fig. 7(ii) are originated from luminescence center originated by gadolinium in O–Si–O complex [37].

Fluorescence emission bands of maximum intensity in the blue green region consist of some other bands of weak intensity at 516 nm, 526 nm and 556 nm observed for the SiO_2:Gd_2O_3 samples. Formation of these bands suggests that the excited electrons have de-excited by their transfer to at least four lower energy levels through vibration or because of energy splitting. Then radiative relaxation occurs and thereby, yield the photons have energy equal to the energy gap between the minima of excited levels and ground state.

Another important result from Fig. 7 is that multi steps annealing at higher temperature (500 °C and 900 °C) led to remarkable decrease in PL intensity. The rare earth clustering could be the possible reason of this type of fluorescence quenching with thermal treatment. The fluorescence quenching effects may be described from more defects like oxygen ion vacancies or E' centers [38,39]. The results are consistent with XRD, FTIR and TEM analysis.

4. Conclusions

The present study demonstrates the versatility of the sol gel method to yield a cubic phase of the sesquioxides in the binary oxide of SiO_2:Y_2O_3 and SiO_2:Gd_2O_3 samples at a low annealing temperature (900 °C) when compared to the temperature (>1400–1600 °C) required for the usual solid-state synthesis. The XRD analysis proved that cubic structure of Y_2O_3 and Gd_2O_3 was well grown within the silica matrix. The average sizes of the nanocrystallites were calculated from the diffraction line width based on the D–S formula, W–H plots and TEM histograms. TEM micrographs confirmed the XRD observations regarding the crystallite/particle size of cubic phase developed in the nano-dimensional powder of rare earth sesquioxides in silica. Influence of multi step annealing on the optical properties is also examined based on PL and UV–vis results. The luminescence intensity is affected by crystalline size/annealing temperature which is confirmed by PL spectra. In the PL spectra, the emission bands are centered in blue–green region. FTIR spectrum of the samples analyzed the functional groups and characteristic bonds of the used precursors.

References

[1] T. Yamaguchi, N. Ikeda, H. Hattori, K. Tanable, J. Catal. 67 (1981) 324.
[2] O.K. Varghese, L.K. Malhotra, L.K. Malhotra, Sens. Actuat., B 53 (1998) 19.
[3] R.K. Goyal, A.N. Tiwari, U.P. Mulik, Y.S. Negi, Compos. Sci. Technol. 67 (2007) 1802.
[4] C.V. Ramana, V.H. Mudavakkat, K. Kamala Bharathi, V.V. Atuchin, L.D. Pokrovsky, V.N. Kruchinin, Appl. Phys. Lett. 98 (2011) 031905.
[5] M.K. Devaraju, S. Yin, T. Sato, Nanotechnology 20 (2009) 305302.
[6] E.J. Rubio, V.V. Atuchin, V.N. Kruchinin, L.D. Pokrovsky, I.P. Prosvirin, C.V. Ramana, J. Phys. Chem. C 118 (2014) 13644–13651.
[7] Y.L. Kopylov, V.B. Kravchenko, A.A. Komarov, Z.M. Lebedeva, V.V. Shemet, Opt. Mater. 29 (2007) 1236.
[8] A.M. Pires, M.F. Santos, M.R. Davolos, E.B. Stucchi, J. Alloys Comp. 344 (2002) 214.
[9] T. Hirai, Y. Asada, I. Komasawa, J. Colloid Interface Sci. 276 (2005) 339.
[10] F. Branda, in: B.S.R. Reddy (Ed.), Advances in Nanocomposite: Synthesis, Characterization and Industrial Applications, 2011, Chapter 14.
[11] C. Cannas, M. Casu, A. Lai, A. Musinu, G. Piccaluga, Phys. Chem. Chem. Phys. 4 (2002) 2286.
[12] S. Xiaoyi, Z. Yuchun, Rare Met. 30 (2011) 33.
[13] N.C. Das, N.K. Sahoo, D. Bhattacharyya, S. Thakur, D. Nanda, J. Appl. Phys. 110 (2011) 063527.
[14] D.D. Martino, N. Chiodini, M. Fasoli, F. Moretti, A. Vedda, A. Baraldi, E. Buffagni, R. Capelletti, M. Mazzera, M. Nikl, G. Angella, C.B. Azzoni, J. Non-Cryst. Solids 354 (2008) 3817.
[15] M. Zhang, L. Xia, Z. Gu, G. Xing, J. Nanosci. Nanotechnol. 13 (2013) 1270.
[16] Rachna, P. Aghamkar, Opt. Mater. 36 (2013) 337–341.
[17] R. Ahlawat, P. Aghamkar, Acta Phys. Pol. A 126 (2014).
[18] S. Mukherjee, P. Dasgupta, P.K. Jana, J. Phys. D: Appl. Phys. 41 (2008) 215004.
[19] N. Dhananjaya, H. Nagabhushana, B.M. Nagabhushana, B. Rudraswamy, C. Shivakumara, R.P.S. Chakradhar, Bull. Mater. Sci. 35 (2012) 519.
[20] Rachna Ahlawat, Int. J. Appl. Ceram. Technol. 1–9 (2014), http://dx.doi.org/10.1111/ijac.12343.
[21] R. Ramamoorthy, S. Ramasamy, D. Sundaraman, J. Mater. Res. 14 (1999) 90.
[22] V.D. Mote, Y. Purushotham, B.N. Dole1, J. Theor. Appl. Phys. 6 (2012) 6.
[23] D.M. Smilgies, J. Appl. Cryst. 42 (2009) 1030.
[24] M. Wilkens, J. Appl. Cryst. 12 (1979) 119.
[25] S. Duhan, P. Agamkar, B. Lal, J. Alloys Comp. 474 (2009) 301.
[26] P.A. Tanner, L.S. Fu, Chem. Phys. Lett. 470 (2009) 75.
[27] G. Kaur, S.K. Singh, S.B. Rai, J. Appl. Phys. 107 (2010) 073514.
[28] L.G. Jacobsohn, M.W. Blair, S.C. Tornga, L.O. Brown, B.L. Bennett, R.E. Muenchausen, J. Appl. Phys. 104 (2008) 124303.
[29] P. Aghamkar, S. Duhan, M. Singh, N. Kishore, P.K. Sen, J. Sol–Gel Sci. Technol. 46 (2008) 17.
[30] X.L. Song, N. Jiang, Y.K. Li, D.Y. Xu, G.Z. Qiu, Mater. Chem. Phys. 128 (2008) 110.
[31] Y.K. Kim, H.K. Kim, D.K. Kim, J. Mater. Res. 19 (2004) 413.
[32] G. Yao, L. Sua, J. Xua, X. Xua, L. Zhenga, Y. Cheng, J. Cryst. Growth 310 (2008) 404.
[33] R. Srinivasan, R. Yogamalar, A.C. Bose, Mater. Res. Bull. 45 (2010) 1165.
[34] F. Gu, S.F. Wang, M.K. Lu, G.J. Zhou, D. Xu, D.R. Yuan, J. Phys. Chem. B 108 (2004) 8119.
[35] N. Zhang, R. Yi, L. Zhou, G. Gao, R. Shi, G. Qiu, X. Liu, Mater. Chem. Phys. 114 (2009) 160.
[36] H.Z. Wu, D.J. Qui, Y.J. Cai, X.L. Xu, N.B. Chen, J. Cryst. Growth 245 (2002) 51.
[37] W. Yi, L. Langsheng, Z. Huiqun, D. Ruiqin, J. Rare Metals 24 (2006) 199.
[38] J. Lin, Y. Han, H. Zhang, Mater. Lett. 54 (2002) 389.
[39] I.K. Battisha, Egypt. J. Sol. 24 (2001) 51.